

## Pairing of a trapped Fermi gas with unequal spin populations

Wenhui Li<sup>a</sup>, G.B. Partridge<sup>a</sup>, Y.A. Liao<sup>a</sup>, and R.G. Hulet<sup>a</sup>.

<sup>a</sup>Department of Physics and Astronomy and Rice Quantum Institute,  
Rice University, Houston, TX 77005, USA

We investigate pairing in a two-component degenerate gas of trapped fermionic  ${}^6\text{Li}$  atoms at a broad Feshbach resonance by *in-situ* imaging of real-space density distributions. From even mixtures of the two spin components, we measured the  $\beta$  factor, describing the universal energy of strongly interacting paired fermions. In uneven spin mixtures, pairing and corresponding phases show a temperature dependence that is consistent with a phase diagram having a tricritical point. At the lowest temperatures, an unpolarized core separates from the excess unpaired atoms by a sharp boundary, which is consistent with a phase separation driven by a first-order phase transition. Moreover, the unpolarized core deforms with increasing polarization, in violation of local density approximation (LDA). In contrast, at higher but still degenerate temperatures, an unpolarized central core remains up to a critical polarization, but does not deform. In this case, the boundaries are not sharp, indicating a partially-polarized shell between the core and the unpaired atoms, consistent with a second-order phase boundary.

### 1. INTRODUCTION

In fermionic systems, the formation of pairs between two constituent components is the essential ingredient of superfluidity and superconductivity. By use of a magnetically-tuned Feshbach resonance, several groups have recently explored the crossover from a BCS superfluid with large Cooper pairs to a Bose-Einstein condensation (BEC) of diatomic molecules in a two spin state mixture of ultracold atomic gases [1–7]. These experiments have advanced our understanding of the strongly interacting regime lying between these two extremes. Another opportunity opened up by experiments with ultracold atoms is the study of possible pairing mechanisms and corresponding phases in systems with mismatched chemical potentials, a topic of active debate. In contrast to the difficulties in generating magnetized superconductors, mismatched Fermi surfaces can be readily realized by creating an imbalance between the populations of two spin components in a gas of trapped ultracold fermionic atoms, as was recently demonstrated [8–11]. New exotic pairing states of matter are predicted for the unbalanced systems, such as the FFLO phase with pairing of nonzero center-of-mass momentum [12,13], the Sarma [14] (or the breached pair [15]) phase, with gapless excitations, and the deformed Fermi surface (DFS) phase [16], where the local Fermi surfaces of the two components deform from spherical to maximize their overlap. In addition, recent theoretical calculations show that phase separation between pairs and excess unpaired atoms is another possible outcome

for a strongly interacting two-component gas [17–21]. These studies of systems with mismatched Fermi surfaces may have important implications for our understanding of unconventional superconductors, nuclei, compact stars, and quantum chromodynamics.

In this paper, we review our experiments on a strongly interacting trapped Fermi gas of  ${}^6\text{Li}$  atoms with *in-situ* images of real-space density distributions.

## 2. APPARATUS AND GENERAL METHODS

Our methods for producing a two-component degenerate Fermi gas with imbalanced populations have been discussed in several previous publications [7,9,11]. A Zeeman slower is used to slow thermal atomic beams of both isotopes of lithium: bosonic  ${}^7\text{Li}$ , and fermionic  ${}^6\text{Li}$ . A magneto-optical trap is used to capture and trap the slowest portion of these pre-cooled atoms. The atoms are next transferred to an Ioffe-Pritchard magnetic trap with a clover-leaf configuration, where they are cooled by rf evaporation. Since spin symmetry prevents spin-polarized fermionic  ${}^6\text{Li}$  from undergoing *s*-wave interactions, the simultaneously trapped and cooled  ${}^7\text{Li}$  atoms function as a thermal reservoir for the  ${}^6\text{Li}$  atoms. Two rf frequencies are used to remove the most energetic  ${}^7\text{Li}$  and  ${}^6\text{Li}$  atoms, and the remaining  ${}^7\text{Li}$  atoms rethermalize through collisions among themselves, while the  ${}^6\text{Li}$  atoms rethermalize through collisions with the  ${}^7\text{Li}$  atoms. At the end of evaporation cycle, the  ${}^6\text{Li}$  atoms are transferred to an optical trap, while the remaining  ${}^7\text{Li}$  atoms are removed by rf spin flips.

The optical trap is formed from a single focused infrared laser beam operating at wavelength of 1080 nm. There is additional confinement provided by magnetic field curvature in the axial direction. The combined optical and magnetic trapping potential is approximately harmonic. In the optical trap, the  ${}^6\text{Li}$  atoms are transferred to the energetically lowest Zeeman sublevel,  $F = 1/2$ ,  $m_F = 1/2$  (state  $|1\rangle$ ), in a nearly uniform bias field of 754 G by a single rf sweep. This sublevel and the second lowest Zeeman sublevel,  $F = 1/2$ ,  $m_F = -1/2$  (state  $|2\rangle$ ), have a broad Feshbach resonance at 834 G [22,23], but neither of them is magnetically trappable. Typically  $3 \times 10^6$  atoms in state  $|1\rangle$  at a temperature  $T \approx 6 \mu\text{K}$  are confined in the trap. To create an *incoherent* spin mixture of state  $|1\rangle$  and state  $|2\rangle$ , a series of 100 saw-tooth frequency ramps are swept through the rf transition resonance between the two states. The use of multiple sweeps ensures that an exact 50/50 mixture may be created even for the case of moderate single sweep efficiency. However, if the rf power is significantly reduced, an imbalanced mixture may also be produced. After preparation of the spin mixture, the atoms are evaporatively cooled by reducing the optical trap depth over a period of approximately 1 s. Thermalization is achieved through collisions between atoms from the two different states. The temperature of the gas can be controlled by evaporating to different final trap depths  $U_0$ . Towards the end of evaporation, we adiabatically sweep the magnetic field to 834 G, where all the experiments in this paper are performed. After a holding time for thermalization and stabilization, states  $|1\rangle$  and  $|2\rangle$  are then sequentially and independently imaged in the trap by absorption using a probe laser beam on resonance with the  $2^2\text{S}_{1/2}$  to  $2^2\text{P}_{3/2}$  atomic transitions specific to each state. The two probes are each 3  $\mu\text{s}$  in duration and are separated in time by 27  $\mu\text{s}$ . The delay is minimized to prevent probe-induced broadening of the second image [9]. The number measurements of the two states,  $N_1$  and  $N_2$ , and global polarization

$P = (N_1 - N_2)/(N_1 + N_2)$ , between 0 and 1, are obtained from analyzing these images. The temperature of the gas is evaluated by fitting the profiles of gases deliberately prepared as  $P = 0$  to fermionic nonzero-temperature Thomas-Fermi distributions.  $\bar{T}$ , the fitted temperature, is expected to be closely related to the actual temperature [5]. Moreover, many properties of the strongly interacting gas can be extracted from real-space density distributions given by these *in-situ* images.

### 3. RESULTS

#### 3.1. Measurement of the $\beta$ factor

When the interaction between two fermionic components is maximally strong (“unitarity” limit), the mean-field contribution of interaction in terms of the local chemical potential can be expressed as  $U_{MF}(\mathbf{r}) = \beta\epsilon_F(\mathbf{r})$  [24], where  $\beta$  is an universal many-body parameter. Since  $\beta$  doesn’t depend on any specifics of the interacting fermions, an accurate determination of  $\beta$  relates to any strongly-interacting fermionic system beyond atomic gases. In our experiments, the unitarity limit is reached by tuning the interaction between two spin components via a Feshbach resonance. In this limit, an unpolarized ( $P = 0$ ) trapped gas is expected to have a reduced chemical potential in the universal form  $E_F(1 + \beta)^{1/2}$ , where the  $\beta$  factor can be determined by measuring its spatial size. Axial density profiles are obtained by integrating the 2D column density distributions along the remaining radial direction, and are insensitive to any residual radial broadening effects [9]. The axial density profiles are then fitted to  $T = 0$  Thomas-Fermi distributions for fermions,  $A(1 - \frac{z^2}{R^2})^{5/2}$ , where  $A$  and  $R$  are adjustable fitting parameters and  $z$  is the axial position. The  $\beta$  factor is given by  $\beta = (R/R_{TF})^4 - 1$  [4,25,26], where  $R_{TF} = (\frac{2k_B T_F}{m\omega_z^2})^{1/2}$  is the axial Thomas-Fermi radius for noninteracting fermions and  $m$  is the atomic mass,  $\omega_z$  is the axial trapping frequency, and the Fermi temperature  $T_F$  is calculated for each state from the measured number  $N_1$  and  $N_2$ . We found that  $R/R_{TF} = 0.825 \pm 0.02$ , giving  $\beta = -0.54 \pm 0.05$ . This value is in excellent agreement with previous measurements [4,5,24,27], but with substantially improved uncertainty. Our measurement is also consistent with  $\beta = -0.58 \pm 0.01$  obtained from two Monte Carlo calculations [18,28,29] and with  $\beta = -0.545$  from a calculation reported in [25].

#### 3.2. Deformation and Phase Separation

Pairing in a two-component gas with unequal populations results in a rich phase diagram that depends on temperature, polarization, and interaction strength of the components in the gas. In this paper, we present experiments performed in the region where interactions are in the unitarity limit.

Shown in Fig. 1 are a series of images corresponding to a range of  $P$  from 0 to 0.95. The difference distributions, obtained by subtracting the minority ( $|2\rangle$ ) from the majority ( $|1\rangle$ ) column density distributions, reveal a central evenly paired core, which we interpreted as a phase separation [11]. In this case, the state  $|2\rangle$  distribution represents the core, while the difference corresponds to the excess, unpaired fermions. The central cuts of column density show that the boundaries between the superfluid core and the polarized normal phase are sharp [11], consistent with the usual convention that phase separation is associated with a first-order phase transition.

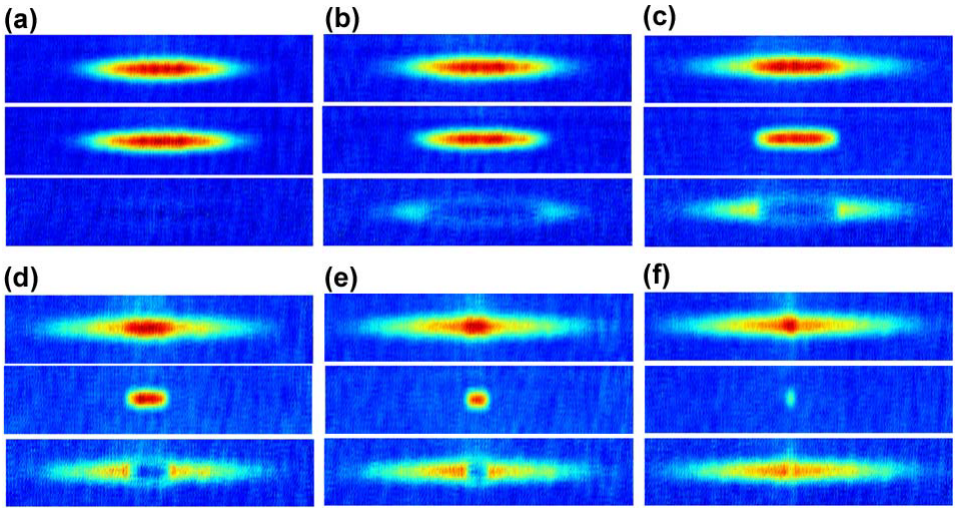


Figure 1. *In-situ* absorption images of a polarized Fermi gas prepared at our lowest temperature of  $\tilde{T} \leq 0.05T_F$ , where  $T_F$  is the Fermi temperature. The radial and axial frequencies at the trap depth are  $\omega_r \simeq (2\pi) 325$  Hz, and  $\omega_z \simeq (2\pi) 7.2$  Hz. From the top to the bottom, the three images in each sub-figure correspond to the column density of state  $|1\rangle$ , state  $|2\rangle$ , and the difference of the two, respectively. The polarizations are (a)  $P = 0$ , (b)  $P = 0.18$ , (c)  $P = 0.37$ , (d)  $P = 0.60$ , (e)  $P = 0.79$ , and (f)  $P = 0.95$ . The field of view for these images is  $1654 \mu\text{m}$  by  $81 \mu\text{m}$ . The displayed aspect ratio is reduced by a factor of 4.4 for clarity. (Reprinted from Ref. [11].)

An apparent, though, unexpected feature is that the radial size of the minority spin remains approximately the same as that of the majority spin, while the distribution of the minority becomes markedly less elongated as  $P$  increases. This deformation results in the bunching of unpaired atoms at the axial poles, and the lack of them in the equatorial shell, as can be seen in the difference distributions in Fig.1. To quantify this deformation, the aspect ratio,  $R_z/R_r$ , for both states are plotted vs.  $P$  in Fig. 2. While the majority state aspect ratio changes little, that of the minority (representing an evenly paired core) decrease by a factor of 10 when going from completely unpolarized ( $P = 0$ ) to completely polarized ( $P = 1$ ).

It is surprising to observe such deformations since they are in violation of local density approximation (LDA). In the LDA, one assumes that all local physics is isotropic, so that the density should follow the isopotential lines of the trap [25,30–35]. Several LDA-violating mechanisms, enhanced by confinement in a high aspect ratio trapping potential, may explain these observations [36,37]. In particular, De Silva and Mueller accounted for surface tension between the normal and superfluid phases, and showed that it can result in deformations of the minority component that are quite similar to those observed here [37].

Cylindrical symmetry allows for the use of an inverse Abel transform to reconstruct the true 3D density distributions  $n(r, z)$  from the 2D column densities. The ratio of the central densities of the two states,  $n_1(0, 0)/n_2(0, 0)$ , obtained from the reconstructed 3D

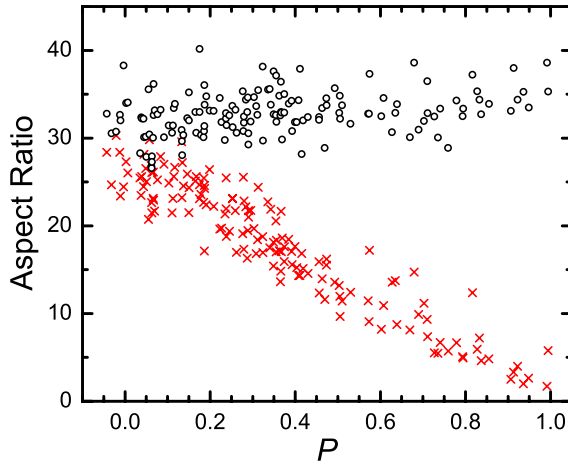


Figure 2. Aspect ratio vs.  $P$ . The ratio of the axial to the radial dimensions,  $R_z/R_r$ , is shown for state  $|1\rangle$  by circles and for state  $|2\rangle$  by crosses. The radial dimension,  $R_r$ , is determined by fitting the column density profiles to zero-temperature, fermionic Thomas-Fermi distributions. The axial distributions are distinctly non-Thomas-Fermi-like, so  $R_z$  is found by a simple linear extrapolation of the column density to zero. The uncertainty in  $P$  is 0.04. The average Fermi temperature is  $T_F \approx 430$  nK, where we define  $T_F = \hbar(\omega_r^2\omega_z)^{1/3}(6N_1)^{1/3}/k_B$ . (Reprinted from Ref. [11].)

distributions, are plotted vs.  $P$  in Fig. 3(a). The figure indicates that the central core remains unpolarized until at least  $P \approx 0.9$ . For  $P > 0.9$ , the increase in  $n_1(0,0)/n_2(0,0)$  may be explained by higher temperatures for these data that arise from inefficiencies in evaporative cooling at very high  $P$ .

### 3.3. Finite temperature observations

Recent theoretical studies on strongly interacting polarized Fermi gases have suggested a phase diagram with three distinct phases connected by a tricritical point [33,38–40]: a phase-separated regime, where an unpolarized superfluid separates from a completely polarized normal gas, a polarized superfluid phase, and a polarized normal phase. The phase-separated phase is preferred at low  $T$ , and is the only phase at  $T = 0$  for nonzero  $P$ . The polarized superfluid phase at low  $P$ , and the normal phase at high  $P$  appear as  $T$  increases, and both of them are expected to have a first-order phase boundary with the phase-separated phase. The three phases meet at the tricritical point, and for higher temperatures, phase-separation is no longer favorable.

We had previously found that phase separation occurred only for  $P > P_c$ , where  $P_c \approx 0.1$  [9]. For  $P < P_c$ , the observations were consistent with a non-phase-separated polarized superfluid. The present data, however, exhibits phase separation for arbitrarily small  $P$ . Since the previous work [9], we have improved the efficiency of the evaporation, and were then able to obtain fitted temperatures that are about half of those previously attained. This temperature-dependent behavior is consistent with a phase boundary between a phase-separated regime and a polarized superfluid (Sarma or breached-pair phase) at nonzero temperature. To further test this hypothesis, we deliberately produced higher

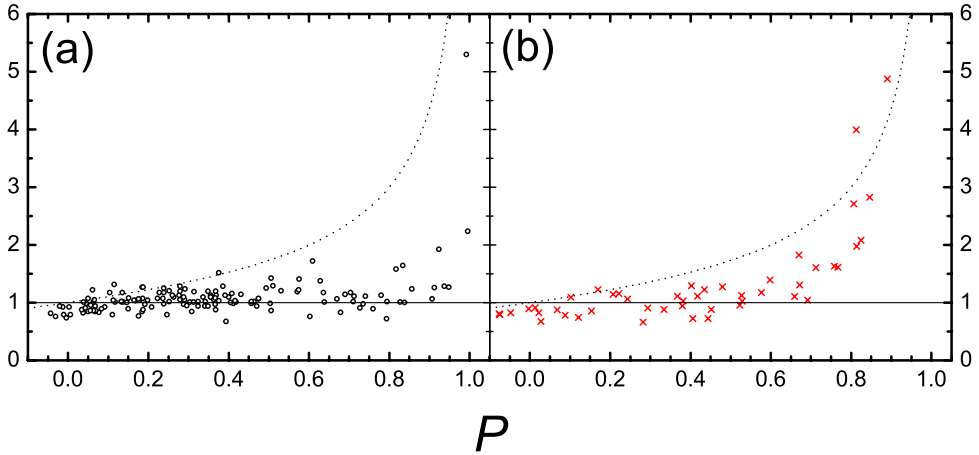


Figure 3. Ratio of the central densities vs. polarization. (a)  $\tilde{T} \leq 0.05 T_F$ , corresponding to the data shown in Fig. 2; (b)  $\tilde{T} \approx 0.2 T_F$ . The dotted lines correspond to  $[(1+P)/(1-P)]^{1/2}$ , the expected central density ratio for a harmonically confined, non-interacting gas at  $T = 0$ . (Reprinted from Ref. [11].)

temperatures by stopping the evaporation trajectory at a higher trap depth, resulting in  $\tilde{T} \approx 0.2 T_F$ . The absorption images of the lower ( $\tilde{T} \leq 0.05 T_F$ ) and higher ( $\tilde{T} \approx 0.2 T_F$ ) temperatures are shown in Fig. 4(a) and 4(c), respectively. It is apparent that the density distributions of the two components of the higher temperature gas show no deformations, in contrast to those of the colder case. Moreover, the higher temperature data does not exhibit the sharp phase boundary between the central core and the normal region, observed at lower temperatures. The absence of deformation can also be seen in the axial density distributions: in the colder case (Fig. 4(b)), the axial difference distribution shows the characteristic double-peaked structure, observed previously [9], while that of the warmer cloud (Fig. 4(d)) exhibits the flat-topped distribution expected for a paired core with no deformation, similar to the observations reported in Ref. [10]. We also extracted the ratio of the central densities of the two states,  $n_1(0,0)/n_2(0,0)$ , for the higher temperature data, and plot it vs.  $P$  in Fig. 3(b). The central densities in this case remain equal until a critical polarization of  $P \approx 0.6 - 0.7$  is reached, which is again consistent with the observations reported in Ref. [10]. These results support the suggestion of a temperature dependent transition between a low-temperature phase separated state and a higher temperature polarized superfluid [39,40].

#### 4. CONCLUSIONS

Ultracold atomic Fermi gases are fascinating for systematic investigations of pairing because of the ability to tune their physical parameters, including interaction strength, polarization, and temperature. They offer clean and controllable experimental systems to study states of matter of relevance to other areas of physics. We have presented a discussion of our experiments on strongly-interacting two-component Fermi gases, especially with unequal spin populations. At the lowest temperatures, we observed pairing

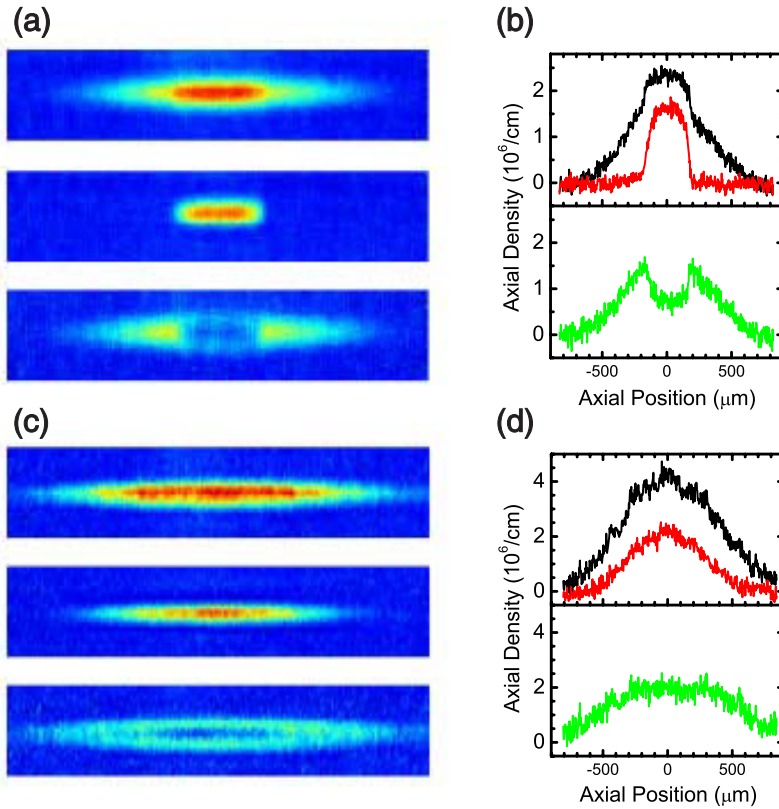


Figure 4. *In-situ* absorption images (left) and integrated profiles (right) for two temperature regimes. (a),(b):  $P = 0.50$ ,  $N_1 = 1.5 \times 10^5$ , with  $\tilde{T} \leq 0.05 T_F$ ; (c),(d):  $P = 0.45$ ,  $N_1 = 3.7 \times 10^5$ , with  $\tilde{T} \approx 0.2 T_F$ . (Reprinted from Ref. [11].)

induced real-space deformations of a polarized Fermi gas in a highly elongated, but still three-dimensional, trap. The sharp phase boundaries between the superfluid core and the completely polarized normal phase are consistent with expectations for a first-order phase transition. At elevated, though, still degenerate temperatures, deformations disappear, and a partially polarized shell is observed between a uniformly paired core and the fully polarized outer shell. These observations suggest the existence of a tricritical point in the phase diagram where the superfluid-normal transition changes from second-order to first-order as the temperature is lowered.

We thank H.T.C. Stoof for helpful discussions, and E. Mueller for helpful discussion and for providing the Abel transform code. This research is supported by the NSF, NASA, ONR, the Welch Foundation.

## REFERENCES

1. C.A. Regal, M. Grenier, D.S. Jin, Phys. Rev. Lett. 92 (2004) 040403.
2. M.W. Zwierlein, C.A. Stan, C.H. Schunck, S.M.F. Raupach, A.J. Kerman, W. Ket-

- terle, Phys. Rev. Lett. 92 (2004) 120403.
3. J. Kinast, S.L. Hemmer, M.E. Gehm, A. Turlapov, J.E. Thomas, Phys. Rev. Lett. 92 (2004) 150402.
  4. M. Bartenstein, A. Altmeyer, S. Riedl, S. Jochim, C. Chin, J. Hecker Denschlag, R. Grimm, Phys. Rev. Lett. 92 (2004) 203101.
  5. J. Kinast, A. Turlapov, J.E. Thomas, Q. Chen, J. Stajic, K. Levin, Science 307 (2005) 1296.
  6. M.W. Zwierlein, J.R. Abo-Shaeer, A. Schirotzek, C.H. Schunk, W. Ketterle, Nature 435 (2005) 1047.
  7. G.B. Partridge, K.E. Strecker, R.I. Kamar, M.W. Jack, R.G. Hulet, Phys. Rev. Lett. 95 (2005) 020404.
  8. M.W. Zwierlein, A. Schirotzek, C.H. Schunk, W. Ketterle, Science 311 (2006) 492.
  9. G.B. Partridge, W. Li, R.I. Kamar, Y.A. Liao, R.G. Hulet, Science 311 (2006) 503.
  10. Y. Shin, M.W. Zwierlein, C.H. Schunk, A. Schirotzek, W. Ketterle, Phys. Rev. Lett. 97 (2006) 030401.
  11. G.B. Partridge, W. Li, Y.A. Liao, R.G. Hulet, Phys. Rev. Lett. 97 (2006) 190407.
  12. P. Fulde, R.A. Ferrell, Phys. Rev. 135 (1964) A550.
  13. A.I. Larkin, Y.N. Ovchinnikov, Sov. Phys. JETP 20 (1965) 762.
  14. G. Sarma, J. Phys. Chem. Solids 24 (1963) 1029.
  15. W.V. Liu, F. Wilczek, Phys. Rev. Lett. 90 (2003) 047002.
  16. A. Sedrakian, J. Mur-Petit, A. Polls, H. Müther, Phys. Rev. A 72 (2005) 013613.
  17. P.F. Bedaque, H. Caldas, G. Rupak, Phys. Rev. Lett. 91 (2003) 247002.
  18. J. Carlson, S. Reddy, Phys. Rev. Lett. 95 (2005) 060401.
  19. D.E. Sheedy, L. Radzihovsky, Phys. Rev. Lett. 96 (2006) 060401.
  20. Z.-C. Gu, G. Warner, F. Zhou, cond-mat/0603091.
  21. H. Hu, X.-J. Liu, Phys. Rev. A 73 (2006) 051603(R).
  22. M. Houbiers, et al., Phys. Rev. A 57 (1998) R1497.
  23. M. Bartenstein, et al., Phys. Rev. Lett. 94 (2005) 103201.
  24. K.M. O'Hara, et al., Science 298 (2002) 2179.
  25. P. Pieri, G.C. Strinati, Phys. Rev. Lett. 96 (2006) 150404.
  26. M.E. Gehm, et al., Phys. Rev. A 68 (2003) 011401(R).
  27. T. Bourdel, et al., Phys. Rev. Lett. 93 (2004) 050401.
  28. J. Carlson, et al., Phys. Rev. Lett. 91 (2003) 050401.
  29. G.E. Astrakharchik, et al., Phys. Rev. Lett. 93 (2004) 200404.
  30. W. Yi, L.-M. Duan, Phys. Rev. A 73 (2006) 031604(R).
  31. C.-H. Pao, S.-K. Yip, J. Phys: Condens. Matter 18 (2006) 5567.
  32. C.-C. Chien, Q. Chen, Y. He, K. Levin, Phys. Rev. A 74 (2006) 021602(R).
  33. F. Chevy, Phys. Rev. Lett. 96 (2006) 130401.
  34. T.N. De Silva, E.J. Muellerr, Phys. Rev. A 73 (2006) 051602.
  35. M. Haque, H.T.C. Stoof, Phys. Rev. A 74 (2006) 011602(R).
  36. A. Imambekov, C.J. Bolech, M. Lukin, E. Delmer, cond-mat/0604423.
  37. T.N. De Silva, E.J. Mueller, Phys. Rev. Lett. 97 (2006) 070402.
  38. R. Combescot, C. Mora, Europhys. Lett. 68 (2004) 79.
  39. M.M. Parish, et al., cond-mat/0605744.
  40. K.B. Gubbles, M.W.J. Romans, H.T.C. Stoof, cond-mat/0606330.